Application of the 3DLD Method for Assessing the Capillary Properties of Self-Fluxing Nickel Alloys and Its Potential Use in the Development of Flame, Additive, and Robotic Cladding Technologies

Authors:
Viktor V. Pankov, PhD, Independent Expert
Sergey V. Pankov, PhD, Independent Researcher
Igor G. Bogorodsky, PhD, Independent Researcher
Vladimir M. Bukin, PhD, Independent Expert
Leonid M. Gurevich †, DSc, Independent Researcher

Contact Information:
Corresponding Author: Vladimir M. Bukin, PhD, Independent Expert, Weston, Connecticut, USA | Email: vmbukin54@gmail.com
Co-author Contact: Viktor V. Pankov, PhD, Independent Expert | Email: erzoff@rambler.ru

Abstract

An evaluation of the structure, chemical, and phase composition of a coating made of the self-fluxing alloy PG-10N-01 was performed. A model for calculating the shape of the coverage was developed. It is shown that the effective capillary constant, determined using a weld bead sample and the 3DLD method, integrally accounts for spreading, diffusion interaction with the substrate material, and crystallization during coating formation. This allows for a more accurate calculation of the specified shape of the deposited bead. Proposals have been formulated regarding the possibility of applying 3DLD technology in robotic cladding and additive manufacturing using self-fluxing alloys.

Keywords: flame cladding, self-fluxing powder alloys, mathematical model, capillary constant, surface profile, weld bead sample, 3DLD technology, additive technologies.

Introduction

The service properties of self-fluxing alloys, such as wear resistance, corrosion resistance, heat resistance, and adhesion strength to the substrate, are largely determined by their shape and thickness, which are specified in the design and technological documentation. These alloys were developed for use as protective coatings applied to the working surfaces of parts by thermal spraying and cladding methods. The development of additive technologies also allows these materials to be used to obtain finished composite products with a complex of necessary properties. Coatings made of self-fluxing alloys with maximum protective properties can only be obtained using technologies that include a fusing operation [1]. The melting temperature interval of self-fluxing alloys (980–1150 °C) [1,2] is significantly lower than the melting temperature of the steels of the parts being protected. This allows the process of coating formation to be considered as consisting of the stages of spreading and crystallization of the self-fluxing alloy melt on the surface of a solid steel substrate.

Various methods and their associated thermal cycles (oxy-fuel flame cladding, electric arc, plasma, and laser cladding) are characterized by different lifetimes of the liquid phase of the coating material. This leads to changes in the chemical and phase composition of the material and the transformation of the operational properties of the coatings. In addition, there is a change in capillary properties that determine the process of shaping the protective layer. The latter circumstance requires the development of a model that allows calculating the shape of the coating formed in various spatial positions, which is particularly relevant for robotic cladding and additive technologies. The 3DLD technology, based on the solution of the Laplace equation, allows calculating the reference shape of the weld seam surface during fusion welding [3,4]. For the first time, the possibility of applying the fundamental equation of the theory of capillarity to calculate the shape of coatings made of the self-fluxing alloy PG-10N-01 at the spreading stage was demonstrated in [5].

To use this equation in engineering calculations, the value of the capillary constant is required. The use of reference values of the capillary constant leads to significant discrepancies between the real and calculated profiles of the forming coating. Under real weld pool conditions, the properties and shape of the coating are significantly influenced by diffusion processes, changes in chemical composition during the interaction of the coating and substrate materials, temperature gradients, cooling rates, and spatial position. All of this must be integrally considered when developing technologies for creating composite materials.

The purpose of this work is to analyze the experience of obtaining and calculating the shape of coatings from the self-fluxing alloy PG-10N-01 by flame cladding [6] and to evaluate the possibility of using self-fluxing alloys to create parts with composite coatings using additive technologies.

Experimental Methodology

The analyzed PhD thesis [6] was completed more than 15 years ago. To study the properties of the coatings, a powder of the self-fluxing nickel alloy PG-10N-01 (analog of Metco 16C-NS), obtained by the atomization method, was used. The powder particles had a spherical shape (Fig. 1a). In some particles, shrinkage pores located in the center were revealed (Fig. 1b). Fractional composition: the +100 μm fraction was not more than 10%, and the rest was 40–100 μm. The chemical composition of the powder according to TUU 322-19-004-96 is: C – 0.6–1.0%, Cr – 14–20%, B – 2.8–4.2%, Si – 4.0–4.5%, Fe – 3.0–7.0%, Ni – base. Hardness: 55–62 HRC.

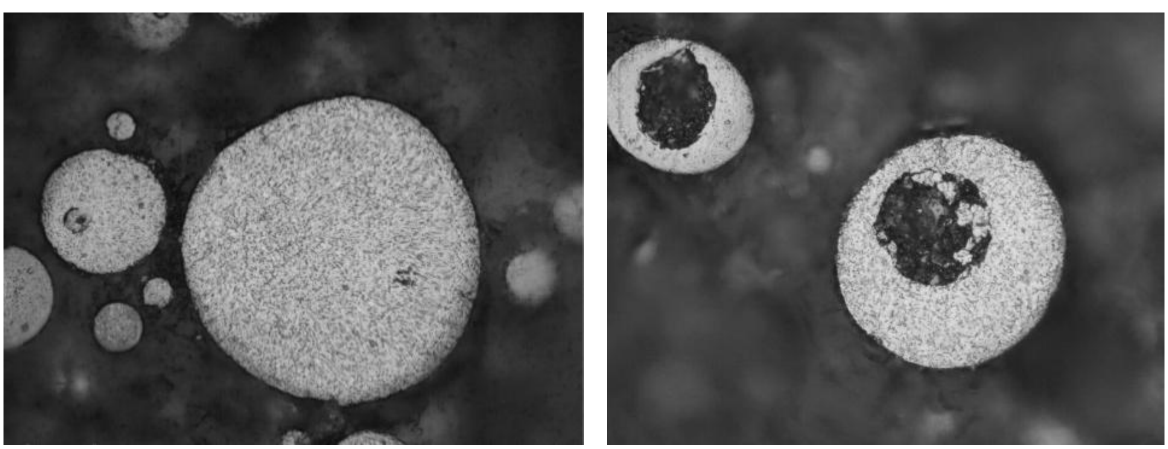

a *b*

Figure 1. Structure of powder particles of the self-fluxing alloy PG-10N-01 (×500×0.5): a – without revealed pores, b – with revealed shrinkage pores.

Visually, a fine-grained structure is identified in the powder, which, according to literature data [7], can be characterized as an eutectic mixture of nickel borides and silicides, chromium carbides and borides with a nickel-based solid solution. The average microhardness of the particles is 5.97 GPa, and the standard deviation from the arithmetic mean is σ = 1.18 GPa. The coating was sprayed and fused with a gas torch using propane-butane mixed with oxygen. During gas-powder cladding of self-fluxing alloys, the lifetime of the liquid phase varies from a few seconds to several tens of seconds, which leads to changes in the structure, phase composition, and properties of the coatings [8]. In this regard, S.V. Pankov's thesis studied the effect of fusing time on the phase composition, microstructure, and capillary constant (ak) of coatings made of the self-fluxing alloy PG-10N-01. The lifetime of the liquid phase was controlled visually and amounted to 10, 20, 30, and 40 seconds. The study of microsections was carried out on an Olympus BX-61 modular microscope. Evaluation of the microhardness of the coatings was conducted on microsections using a PMT-3M microhardness tester. The phase and chemical composition of the coatings were determined using a Dron 3 diffractometer and a Niton Xl3t metal analyzer.

Results of the Evaluation of the Effect of Liquid Phase Lifetime on the Structure and Properties of the Coating from the Self-Fluxing Alloy PG-10N-01

The microstructure of the powder coatings of the self-fluxing alloy PG-10N-01 is multi-phase. According to X-ray diffraction data, the completely fused coating contains eutectic mixtures of a nickel-based solid solution with chromium carbides and silicides, as well as nickel borides. With an increase in the fusing time, coarsening of the structure occurred, accompanied by a transformation from highly dispersed eutectic structures with small excess borides and carbides (Fig. 2a) at a fusing time of 10 seconds to the appearance of randomly oriented dendrites (Fig. 2b) at a fusing time of 40 seconds.

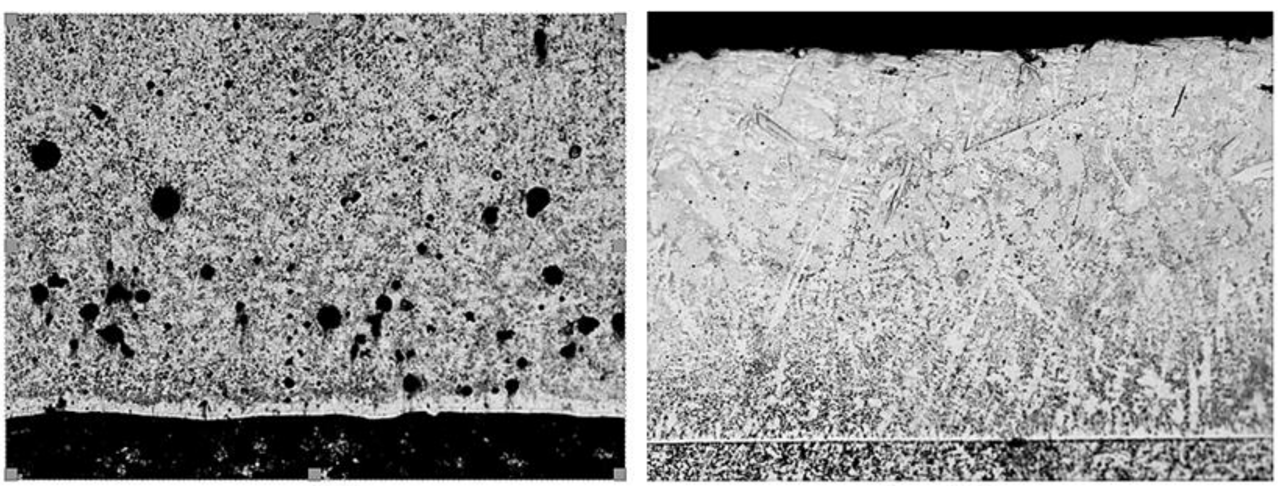

a x100 b x100

Figure 2. Microstructure of coatings at a fusing time of 10 seconds (a) and 40 seconds (b).

The porosity of the coating decreases (Fig. 3), and large needle-like (Fig. 4c) and polygonal (Fig. 4d) excess crystals with high hardness appear in the structure.

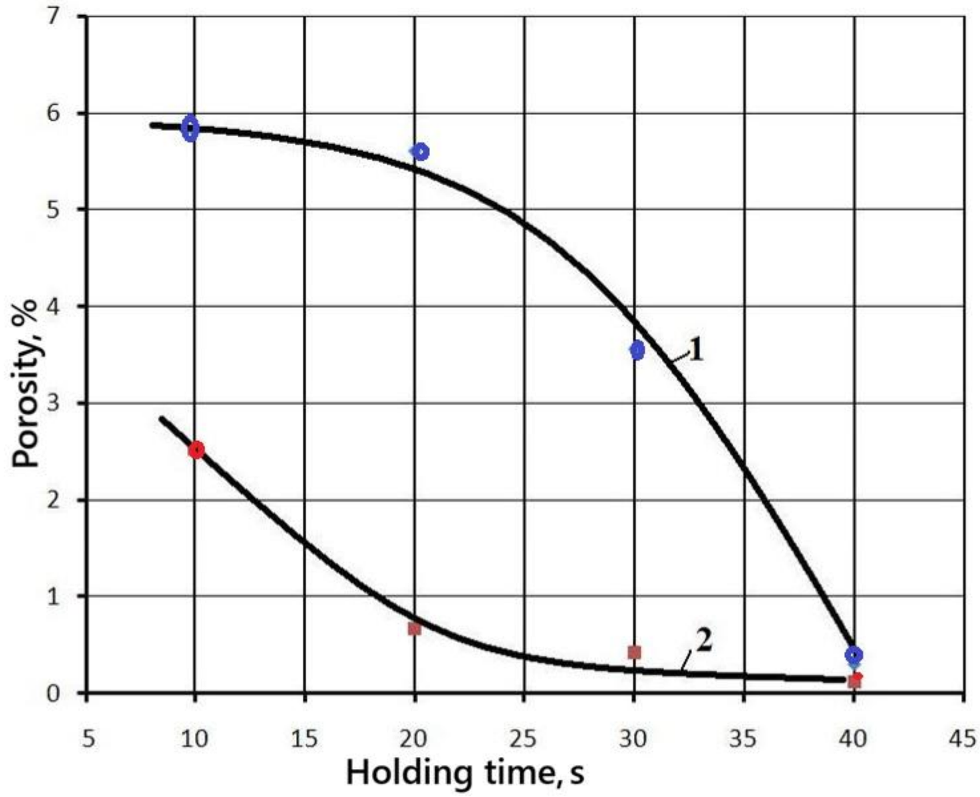

Figure 3. Dependence of porosity on the coating fusing time: 1 – coating thickness 1.0–1.5 mm; 2 – coating thickness 0.8–1.0 mm.

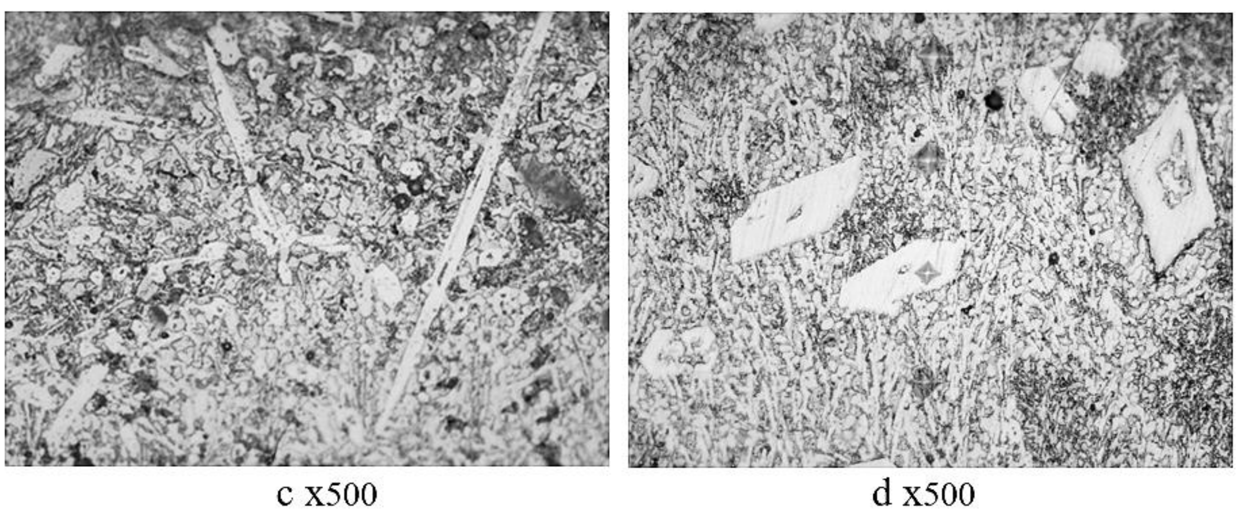

Figure 4. Microstructure of coatings at a fusing time of 40 seconds (c, d).

The microhardness of the coatings increases with distance from the bonding interface with the steel. An increase in the fusing time leads to a decrease in average microhardness values from 11 to 4.5 GPa (Figure 5).

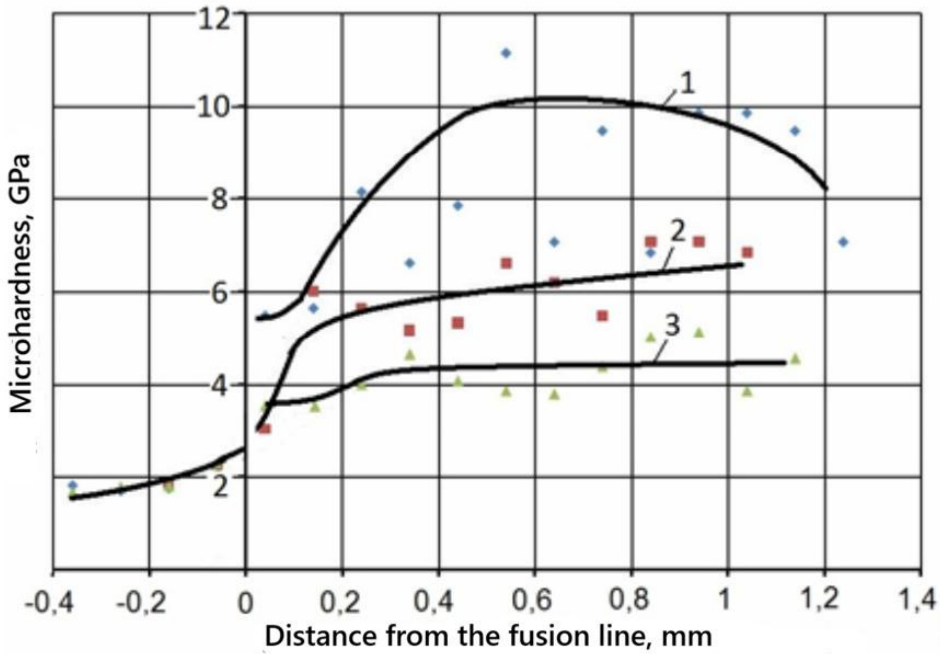

Figure 5. Microhardness distribution across the coating thickness at various fusing times: 1 – 10 seconds, 2 – 20 seconds, 3 – 40 seconds.

To eliminate the influence of the dissolution of the steel substrate on the microstructure and microhardness of the coating, the microstructure of solidified droplets formed on a non-wettable ceramic substrate with liquid phase lifetimes of 10, 20, and 40 seconds was investigated. With an increase in the holding time from 10 to 40 seconds, coarsening of the droplet structure occurred from fine-grained with a high volume content of eutectic to coarse-grained with needle-like and polygonal crystals (Fig. 6).

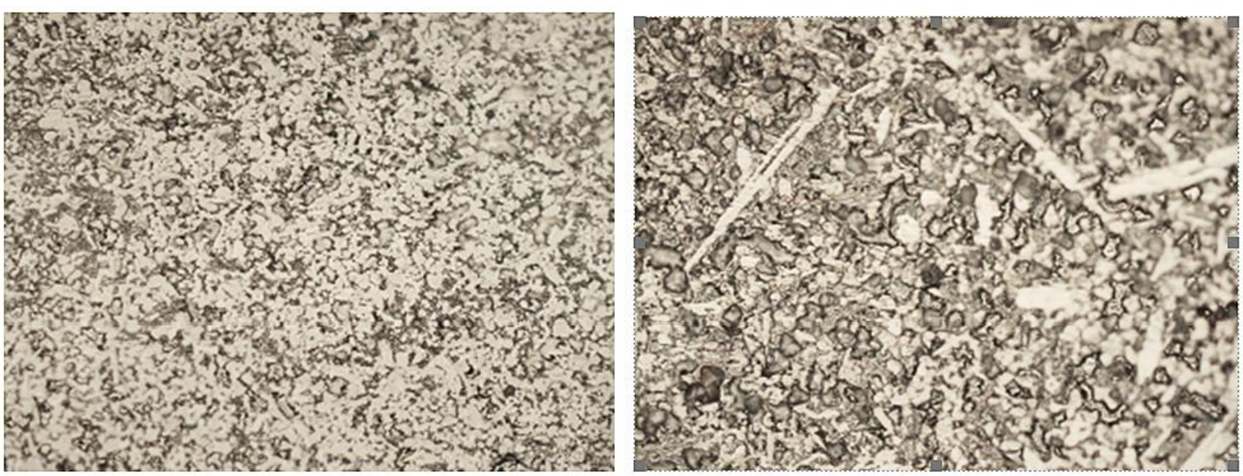

Figure 6. Microstructure of droplets crystallized on a ceramic substrate: a – 10 s, b – 20 s.

Similar microstructures were observed in coatings applied to the steel base (Fig. 4). Thus, the coarsening of the structure is determined only by the temperature-time parameters of the powder fusing. Evaluation of the microhardness distribution across the cross-section of the droplets crystallized on the ceramic substrate showed that it practically does not change with different lifetimes of the liquid phase and remains within 8.5–11 GPa.

The appearance of an intermediate layer with a modified microstructure at the interface between the cladded coating and the steel substrate was observed previously and explained by the influence of iron dissolved in the coating [9]. To verify this statement, an investigation of the content of three elements (Ni, Cr, and Fe) on the resulting surface was performed using a NITON XL3t portable X-ray fluorescence alloy analyzer. The obtained results of the chemical analysis of the iron content across the thickness of the cladded coatings (Fig. 7) confirm the previously made assumption about the dissolution of the steel base in the cladded coating.

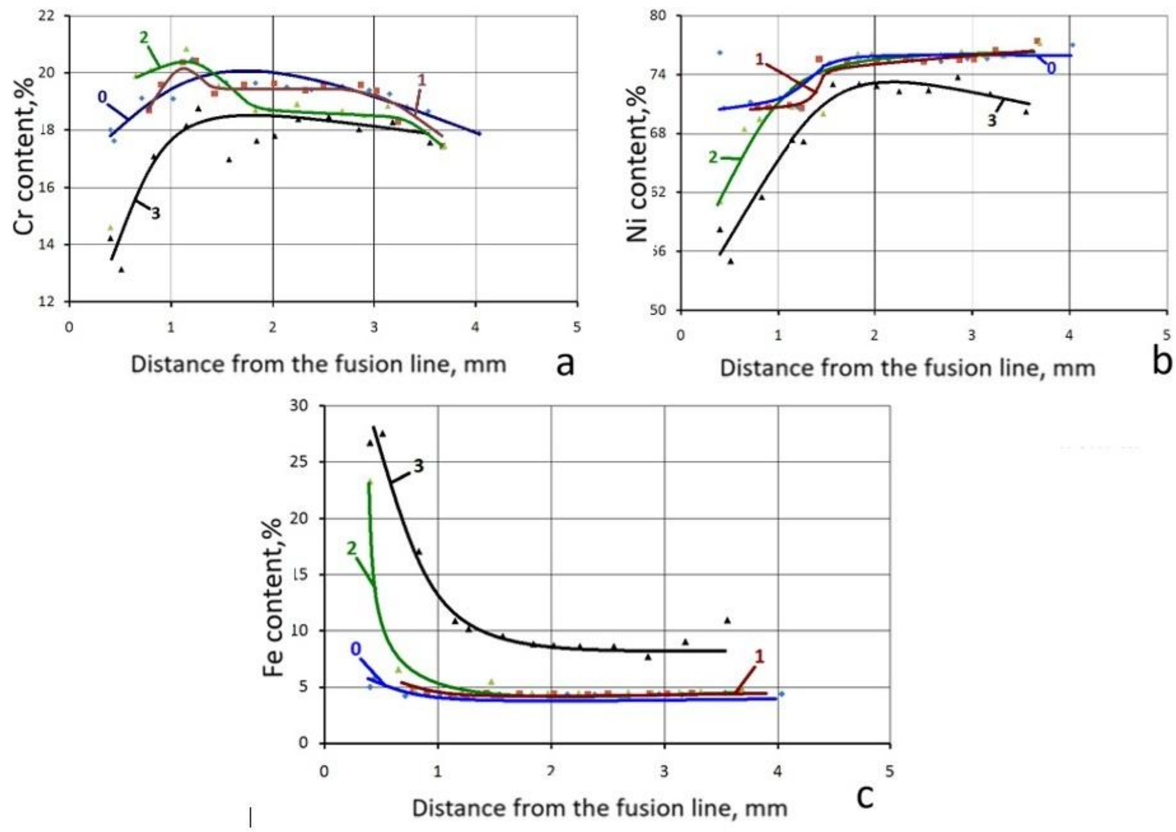

Figure 7. Change in Cr (a), Ni (b), and Fe (c) content across the thickness of the cladded coatings at various lifetimes of the liquid phase: 0 – fusing time 10 seconds; 1 – fusing time 20 seconds; 2 – fusing time 30 seconds; 3 – fusing time 40 seconds.

An increase in the lifetime of the liquid phase up to 40 s led to: a decrease in the nickel content near the fusion line to 55 wt.% (Fig. 7b), and chromium to 13 wt.% (Fig. 7 a)., and an increase in the iron content near the fusion line up to 27 wt.% and up to 10 wt.% across the entire thickness of the cladded coating (Fig. 7 c).

The microstructure of flame cladded powder coatings of the self-fluxing alloy PG-10N-01 is multi-phase. Analysis of the diffraction pattern decoding results of the initial powder (Fig. 8a) allowed identifying the following phases: a solid solution based on Ni (period 2.038 Å, relative intensity 1) and Ni3B (tabulated value of the period 2.03 Å, relative intensity 1). In addition, the following phases are reliably identified in the structure of the self-fluxing alloy powder: a solid solution based on Ni, Ni3B, CrB. The following phases were presumptively identified: Cr7C3, Cr23C6, Ni3Si. Detailed metallographic studies and X-ray phase analysis of the nickel-chromium-boron-silicon alloy PG-10N-01 conducted by the author [9] also indicate the presence of the aforementioned phases.

A change in the chemical composition of the coating as a result of an increase in the duration of the liquid phase existence also leads to a change in their phase composition. According to X-ray diffraction data, even with a melt lifetime of 5 s, the phase composition differentiates and differs from the phase composition of the initial powder (Fig. 8a). On the free surface of the coating (Fig. 8b), the following phases are reliably detected: a solid solution based on nickel, nickel boride Ni3B, nickel silicide Ni3Si, chromium borides CrB, and chromium carbides Cr23C6 and Cr7C3.

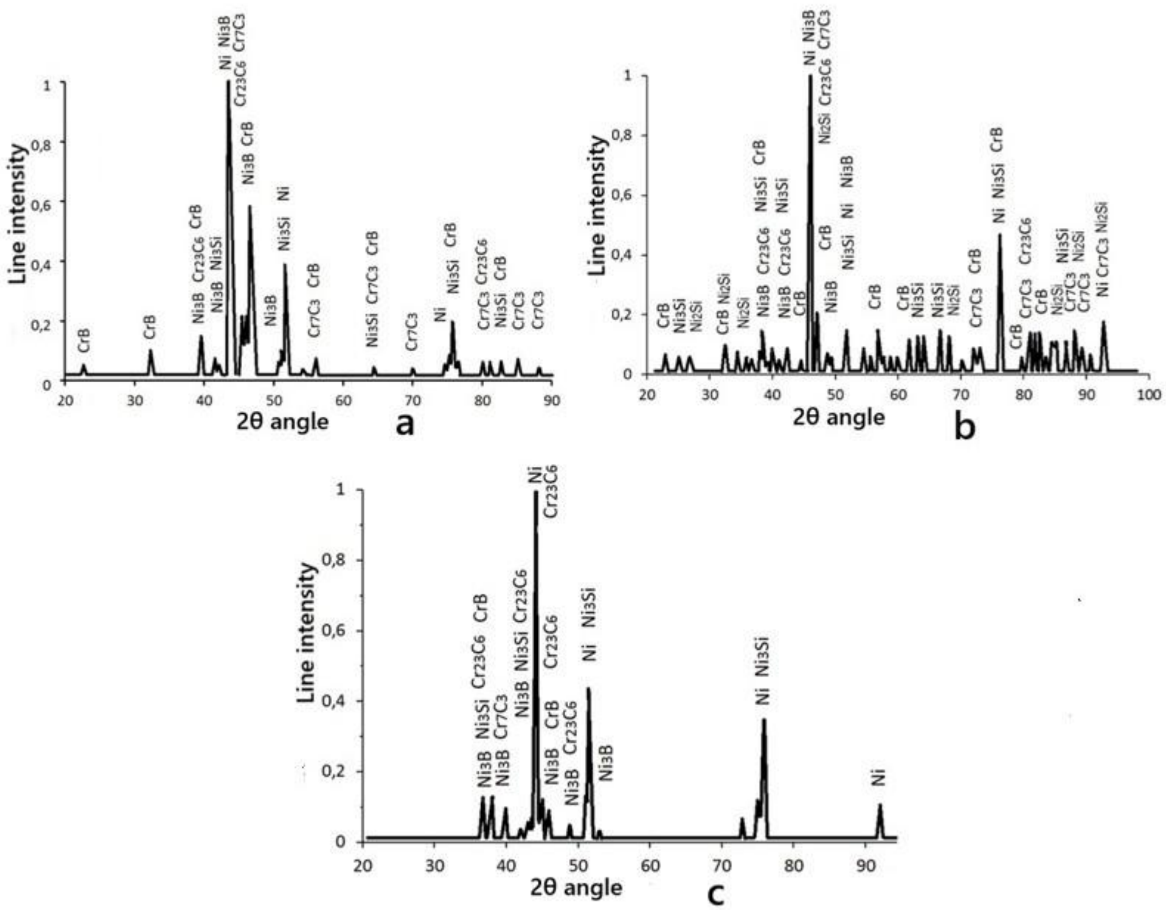

Figure 8. X-ray diffraction patterns: particles of powder PG-10N-01 (a); coating surface at a fusing time of 5 seconds (b) and a fusing time of 40 seconds (c).

The existence of a liquid phase during coating cladding for 40 seconds, accompanied by the dissolution of the steel base, led to a transformation of the phase composition (Fig. 8c). The main phase giving the most intense peaks is a nickel-based solid solution in which up to 10% iron is dissolved. The role of strengthening phases is played by nickel borides Ni3B and chromium borides CrB, and a carbide of the (Cr, Fe)23C6 type; however, their volume content is significantly lower than in the initial powder (Fig. 8a) and coatings formed at liquid phase lifetimes of 10 and 20 seconds.

Conclusions of Section

1. In the process of flame spraying with fusing of the self-fluxing alloy PG-10N-01, the lifetime of the liquid phase determines the structure and porosity of the coating. With an increase in the lifetime of the liquid phase, coarsening of the coating microstructure occurs up to the appearance of randomly oriented dendrites and large inclusions of carboborides, a decrease in porosity from 2.5–6% at 10 s to 0.1–0.3% at 40 s, and a decrease in microhardness from 11 GPa to 4.5 GPa, respectively, associated with the dissolution of iron in the coating material.

2. The process of dissolution of the steel base in the melt of the self-fluxing alloy leads to the formation of structural and chemical heterogeneity with the formation of a zone near the interface, in which the iron content increases to 27.5%, and the content of chromium and nickel decreases to 13% and 55%, respectively. It is shown by X-ray diffraction methods that with an increase in the fusing duration, a coating is formed in the structure of which the volume fraction of strengthening phases (carbides, borides, and silicides) decreases with a simultaneous increase in the content of the nickel-based solid solution.

Model for Assessing the Coating Surface Shape

To control the cladding process and predict the quality, shape, and properties of self-fluxing coatings, it is necessary to create a model of coating formation. For the first time, the possibility of applying the fundamental equation of the theory of capillarity [10] to calculate the shape of coatings applied by thermal spraying followed by fusing (flame cladding with fusing) from the self-fluxing alloy PG-10N-01 at the spreading stage was demonstrated in the work of S.V. Pankov [5,6]. The calculation scheme for determining the shape of the interface surface of the fused coating from a self-fluxing alloy powder is shown in Figure 9.

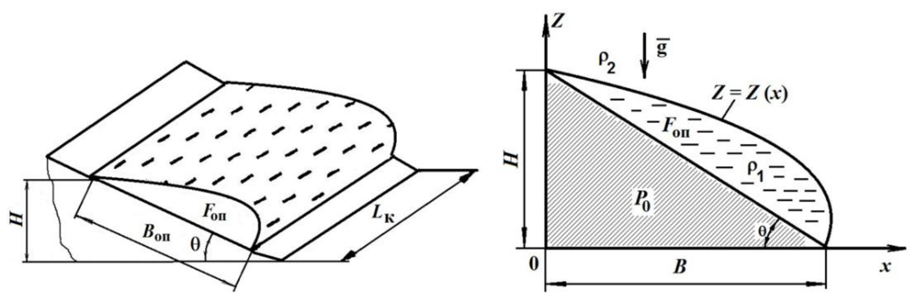

Figure 9. Calculation scheme for determining the equilibrium shape of the interface surface of fused self-fluxing alloy powder on inclined substrates: a – physical model, b – calculation scheme for constructing a mathematical model: Fop – area of the fused coating; P0 – fictitious area of the substrate metal; Lk – length of the cladded bead; Bop – width of the coating bead; ρ1 density of the coating material; ρ2 – density of the gas medium; Θ – tilt angle of the substrate.

In mathematical modeling of the process of forming the surface of a coating cladded using a gas torch flame as a heat source, the following assumptions and simplifications were made:

1. The process of coating formation is stable, which makes it possible to consider the quasi-static equilibrium of the liquid phase, and the surface of the liquid phase in the crystallization zone is a dynamically stable formation.

2. The temperature of the molten self-fluxing alloy and the surface temperature of the substrate are in a state close to isothermal equilibrium.

3. The entire surface of the pool crystallization zone is isothermal, which allows excluding thermocapillary motion from consideration.

4. The surface of the liquid phase crystallization zone is cylindrical, that is, this region of the liquid phase has curvature in only one direction - in the cross-section perpendicular to the direction of movement of the heating source. The adoption of this assumption leads to the constancy of the shape and dimensions in any cross-section of the liquid phase in the crystallization area and allows solving a planar problem instead of a volumetric one.

5. The surface of the crystallization zone retains the shape adopted under the action of gravity and surface tension forces of the liquid phase.

The accepted assumptions allow reducing the determination of the shape of the liquid phase crystallization zone of the fused coating to solving the problem of finding the equilibrium shape of a cylindrical isothermal surface of a capillary liquid in a uniform field of mass forces.

When solving the problem of determining the shape of a protective coating by the method of calculus of variations for a cylindrical free interface surface, the differential equation of equilibrium of an interface surface under the action of interfacial tension and gravitational forces was used:

$$\frac{Z^{//}(x)}{\left\{1+\left[Z^{/}(x)\right]^2\right\}^{3/2}}-\frac{Z(x)}{a_{\kappa}^2}+\frac{1}{R_0}=0\,, \qquad (1)$$

where: Z(x) is a function describing the shape of the interface surface of the liquid phase of the protective coating; $0 \le x \le B$ (x = 0 is the left boundary of the protective coating, x = B is the right boundary of the protective coating); ak is the capillary constant; R_0 is the radius of curvature of the curve Z = Z(x) at the point x = 0.

For the numerical solution of the differential equation (1) at given values of B, Fop, ak, the shape of the interface curve is constructed. When calculating the shape of the coating according to equation (1), it is necessary to know the value of the capillary constant ak, which depends only on the physical properties (density and surface tension) of the contacting phases and is represented by the following relation:

$$a_{\kappa}=\sqrt{\frac{\sigma}{g(\rho_1-\rho_2)}}\,. \qquad (2)$$

where: σ is the surface tension at the interface; ρ1 and ρ2 are the densities of the contacting phases; g is the acceleration of free fall.

Values of the capillary constant for most widespread powders of self-fluxing alloys are absent in the reference literature. Therefore, in this work, using 3DLD technology, a method was developed and the values of the effective capillary constant of some self-fluxing alloys were determined: PG-10N-04 (Analog of Eutalloy 10224), PG-10K-01 (Analog of Eutalloy PE 8210), NChP-3 (Analog of Eutalloy PE 8418), used for coating application.

Method of Determination and Results of Evaluation of the Capillary Constant of Self-Fluxing Alloys

To determine the interfacial properties of capillary liquids, a large number of methodologies have been developed, but their use leads to conflicting results; thus, the values of interfacial tension obtained for the same liquid metals by different methodologies differ by 20%–30% [11,12].

The static sessile drop method is considered the most reliable [13]. When using it, a drop of melt lying on a substrate made of non-wettable material is photographed.

and two of its dimensions are determined from the photograph: the maximum diameter d and the distance h from the top of the drop to its plane having the maximum diameter (Fig. 10).

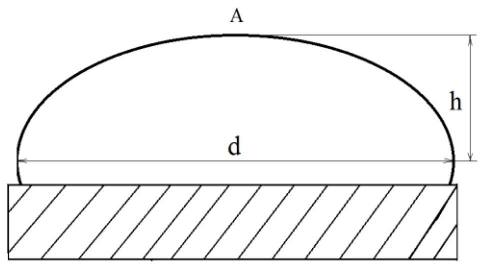

Figure 10. Scheme for determining surface tension by the sessile drop method.

Knowing these dimensions allows finding the value of surface tension from graphs or tables using a criteria equation of the form $\frac{a^2}{d^2} = f\left(\frac{d}{2h}\right)$ [14]. To increase accuracy, it is necessary to photograph the drop in a molten state in a vacuum, since in an oxidizing atmosphere an oxide film forms on the surface of the drop, distorting its shape, and during melt crystallization, the shape and dimensions change due to volume reduction. When measuring the dimensions of drops solidified in air, these two factors can lead to a significant error in determining the surface tension of a liquid. The model for predicting the coating profile developed in [5,6] also does not account for the change in the shape of the crystallizing melt of a self-fluxing alloy with the formation of oxide films; therefore, for calculating the coating shape, it is necessary to use not the true value of the capillary constant, but its effective value, which takes into account the distorting effects during metal solidification. In this work, to obtain effective values of ak, the sessile drop method was used with measurement of drops of various sizes of self-fluxing alloys weighing 4–8 g crystallized in an air atmosphere on a ceramic substrate (Fig. 11).

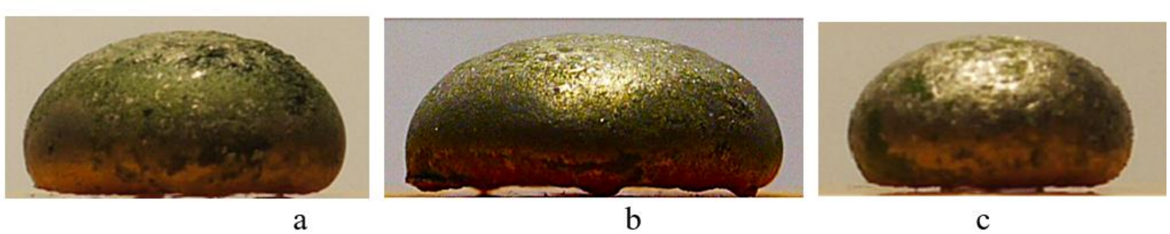

Figure 11. Drops of various sizes (d/h) made of self-fluxing powder alloy PG-10N-01, obtained on a ceramic substrate: a – 10.07/3.61; b – 13.85/4.55; c – 11.56/3.69.

In parallel, the value of ak was determined by solving the inverse problem using the developed mathematical model based on the shape of the applied coating bead (weld bead sample). In the weld bead sample method, a powder coating up to 3 mm thick was cladded onto the surface of a steel substrate measuring 100x15x8 mm (Fig. 12).

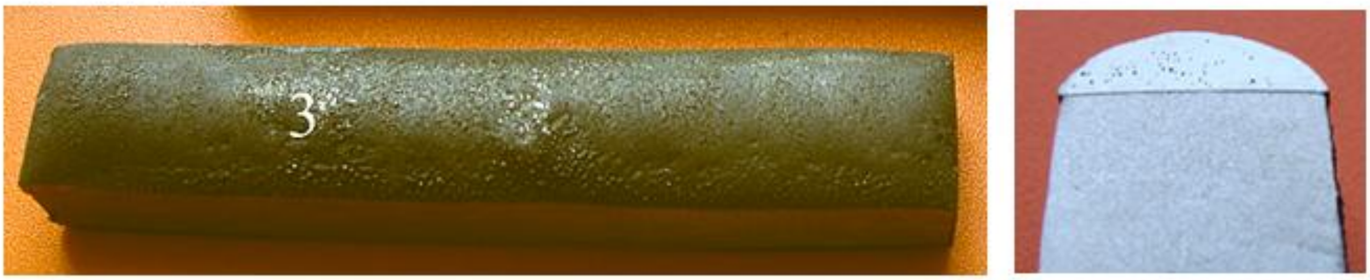

a b

Figure 12. Sample of a weld bead probe from PG-10N-01 powder (a) and its macrosection (b).

The macrosection (Fig. 12b) cut in the plane perpendicular to the direction of movement of the cladding torch was scanned with a resolution of 1200 dpi, and the digitized profile of the solidified coating was digitized from the obtained digital photographs by measuring its height across the specimen width with a step of 0.2 mm, using the AnalySiS software package from Olympus Soft Imaging Solutions GmbH (Germany). The obtained array of experimental digital data characterizing the shape of the fused coating with a bead width B and area Fop was processed by the 'Spray Bead' program.

The sought effective capillary constant value was performed by selection from a family of integral curves obtained by numerical solution of differential equation (1) with variation of ak values, maximally close to the obtained data array of the experimental bead cross-section profile. The sum of squared differences between the experimental and model-calculated coating profile height values was used as a selection criterion. For all values of xi of each of the calculated families of integral curves, the difference ΔZ_i of the experimental Z_i^e and calculated Z_i^p values of the coating profile heights at the coordinate xi was evaluated, as well as the sum of squared differences $\sum(\Delta Z_i)^2$. As the effective capillary constant, the effective value of ak was chosen, the use of which allowed obtaining a curve with the minimum value of the sum of squared differences during the numerical solution of differential equation (1):

$$m = \min\left[\sum_{i=1}^{n}(\Delta Z_i)^2\right] \quad (3)$$

A graphical representation of this procedure is shown in Fig. 13.

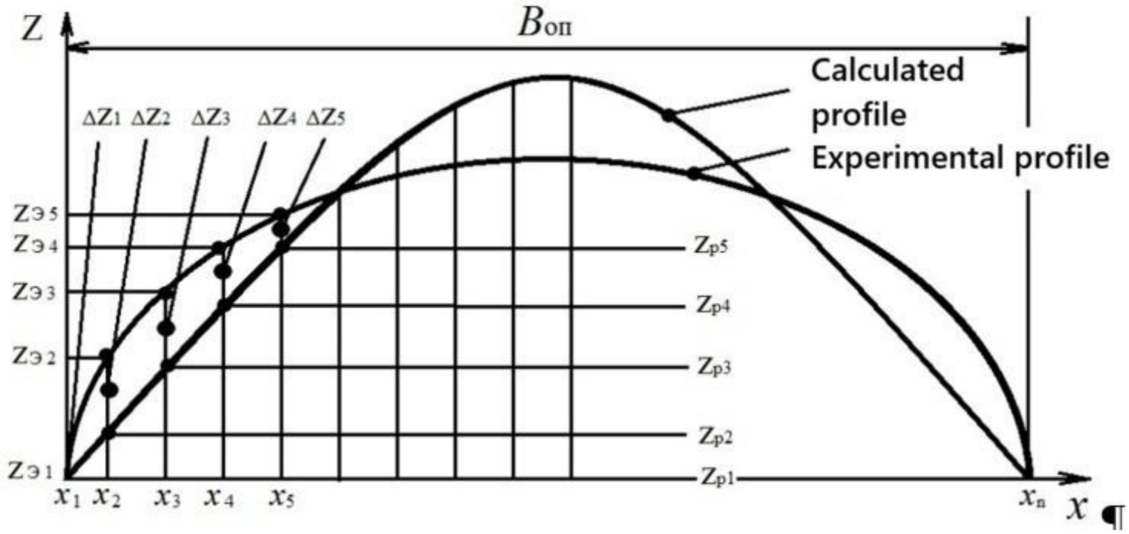

Figure 13. Calculation scheme for determining a_{k}.

The value of ak determined by the sessile drop method was 3.9–4.4 mm. The value of ak calculated by the proposed weld bead sample method was 2.9–2.97 mm. Comparison of the ak values obtained by the two different variants shows that when using the sessile drop method, the ak values are 35%–45% higher than the results obtained by the weld bead sample method. This is probably due to the fact that the method of a drop lying on a ceramic substrate does not account for the dissolution of iron and, consequently, changes in capillary properties. Therefore, for practical purposes (calculating the bead profile), it is advisable to use the values of the capillary constant ak obtained using the developed weld bead sample method, which is significantly more accurate and closer to the real conditions of coating formation (Fig. 14).

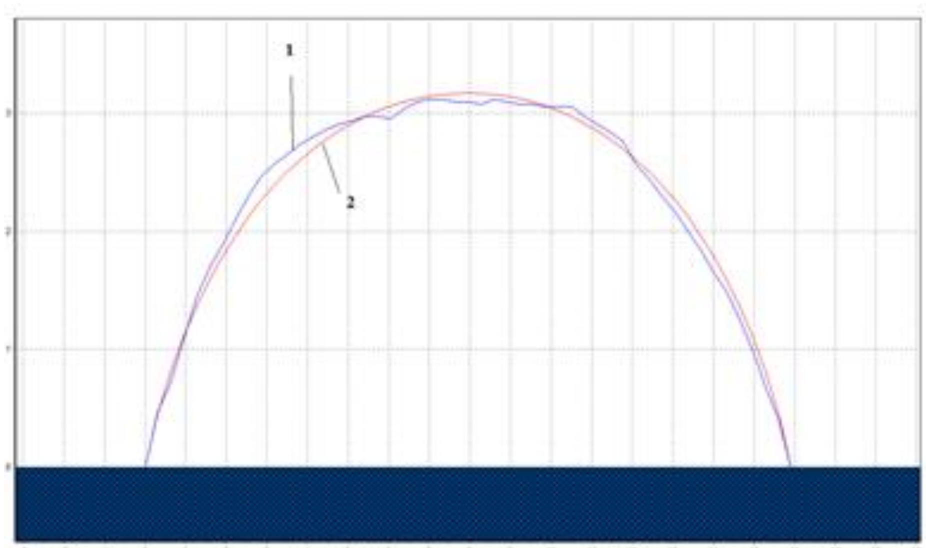

Figure 14. Experimental (1) and calculated (2) curves.

The values of the effective capillary constant ak of melts of widely used self-fluxing alloys based on cobalt, nickel, and copper obtained in [5], determined by alternative methods of the sessile drop and weld bead sample, are given in Table 1

Table 1. *Values of the effective capillary constant of self-fluxing alloy melts.*

Method of Determination	PG-10K-01 (Analog of Eutalloy PE 8210)	PG-10N-01 (Analog of Metco 16C-NS)	PG-10N-04 (Analog of Eutalloy 10224)	NPCh-3 (Analog of Eutalloy PE 8418)
Sessile drop	4.09	4.16	3.84	3.33
Weld bead sample	2.99	2.91	2.24	2.43

Comparison of the values of the effective capillary constant of the melts showed that the sessile drop method gives ak values 35%–70% higher than the weld bead sample method. This may be due to the difference in effects associated with the differentiation of substrate wettability, heat removal conditions during crystallization, and the possibility of iron saturation of the melt contacting the steel substrate. In this regard, an evaluation of the influence of the holding time on the value of the capillary constant of the self-fluxing alloy PG-10N-01 was performed. Calculation of the capillary constant showed that with an increase in the lifetime of the liquid phase, the value of ak decreases from 3.46 mm to 2.97 mm (Fig. 15).

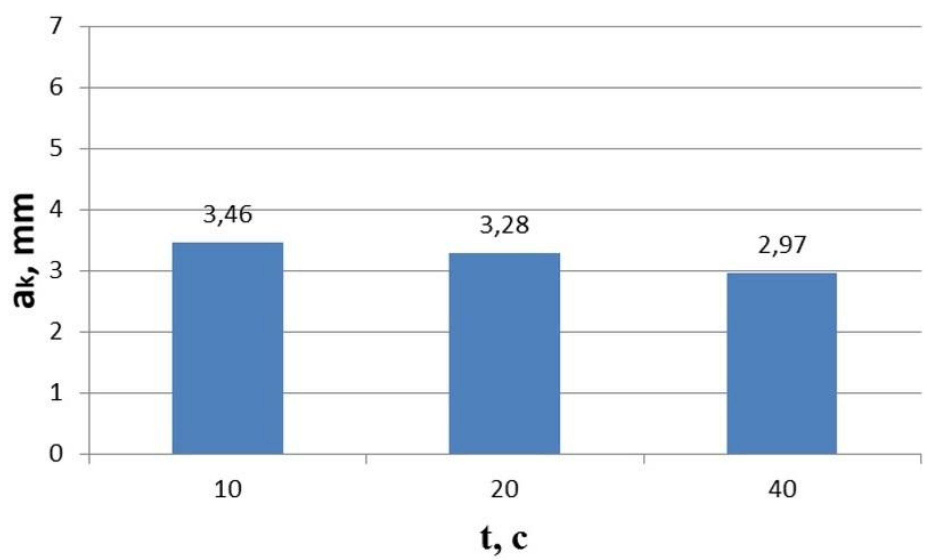

Figure 15. Dependence of the capillary constant a_k on the lifetime of the coating liquid phase obtained on a steel substrate.

To eliminate the influence of the dissolution of the substrate material, an experiment was conducted to form a melt drop on a ceramic substrate. It was established that in this case, the value of ak practically does not change, but is higher than that of coatings obtained on a steel substrate (Fig. 16).

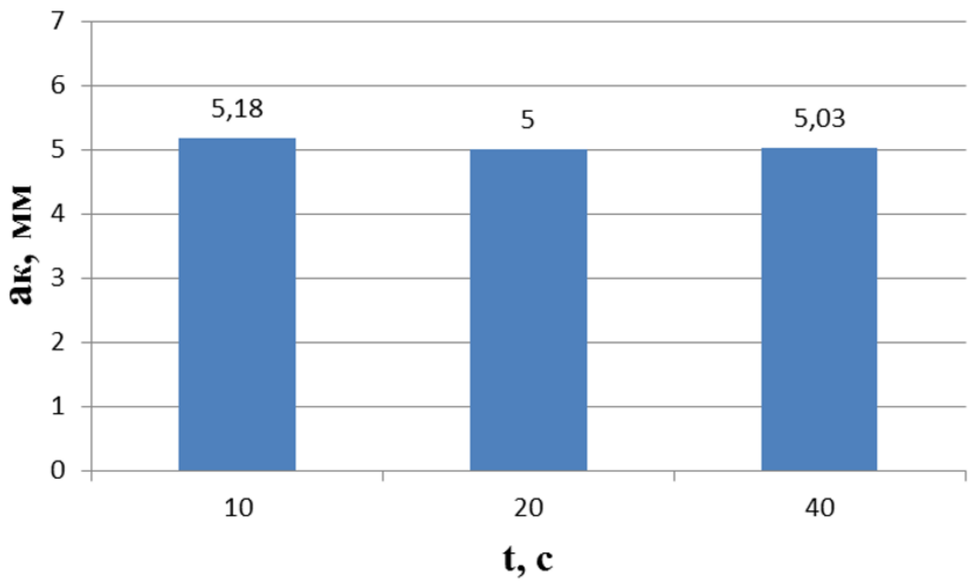

Figure 16. Dependence of the capillary constant a_k on the lifetime of the coating liquid phase obtained on a ceramic substrate.

Conclusions of Section

Thus, the development of a physical-mathematical model for calculating the coating shape allows determining the coating shape and its capillary properties by calculation. Determining the effective capillary constant for various materials and a specific technological mode ensures good agreement (Fig. 14) of the calculated model with the geometry of a real weld. This makes it possible to predict the coating shape for other spatial positions, warn about the risk of defects, and control the coating cladding process.

Analysis of Results and Development of Proposals for Using the 3DLD Method for Robotic Cladding and Additive Technology

The experimentally established result of a drop in the effective capillary constant of the PG-10N-01 alloy from 3.46 mm to 2.97 mm with an increase in the lifetime of the liquid phase from 10 to 40 seconds finds strict confirmation in the structural-chemical transformations of the melt.

At the minimum holding time (5–10 seconds), diffusion processes at the 'coating–substrate' interface are limited. X-ray diffraction analysis shows that the structure is dominated by a high volume fraction of dispersed strengthening phases — nickel and chromium carbides, borides, and silicides, providing a microhardness at the level of 10 GPa. The high interfacial energy of this clean heterogeneous system maintains the convex shape of the bead meniscus, which is captured by the inverse calculation of the Laplace equation as the maximum value of the capillary constant ak = 3.46 mm. At the same time, the porosity of the layer is 2.5–6%, indicating insufficient time for complete degassing of the pool.

With an increase in the liquid phase lifetime to 40 seconds, the process of dissolution of the steel base in the nickel melt enters an active phase, forming a pronounced structural-chemical heterogeneity. The iron content in the zone near the interface increases to 27.5%, while the concentration of chromium and nickel drops to 13% and 55%, respectively. This metallurgical shift leads to the dissolution of the volume fraction of borides and silicides with the simultaneous formation of a coarse-dendritic nickel-based solid solution, which is accompanied by a drop in microhardness to 4.0 GPa.

From the standpoint of capillary theory, the saturation of the melt with iron up to 27.5% and the disappearance of refractory borides cause a sharp drop in the surface tension of the liquid metal. The pool acquires high fluidity, and the bead meniscus flattens asymmetricly, which is contactlessly registered by an optical method as a drop in the constant a_kef to 2.97 mm. At the same time, the long lifetime of the liquid phase ensures virtually complete degassing of the melt, reducing porosity to a record 0.1–0.3%.

Thus, it is experimentally proven that the dynamic change in the capillary constant is a direct geometric reflection of fundamental metallurgical processes — phase rearrangement and diffusion dissolution of the substrate. This allows using the geometry of the solidifying meniscus as a tool for controlling the chemical composition, Young's contact angles, shape defects, and layer porosity of the coating.

The developed physical-mathematical model makes it possible not only to predict the coating shape but also allows determining the effective capillary constant from the surface shape of a real cladded bead. This contributes to an accurate calculation of the cladded profile of the coating both on a flat (Fig. 16) and on an inclined surface (Fig. 17) and creates a basis for the development of automated technologies for controlling the cladding process of self-fluxing alloys.

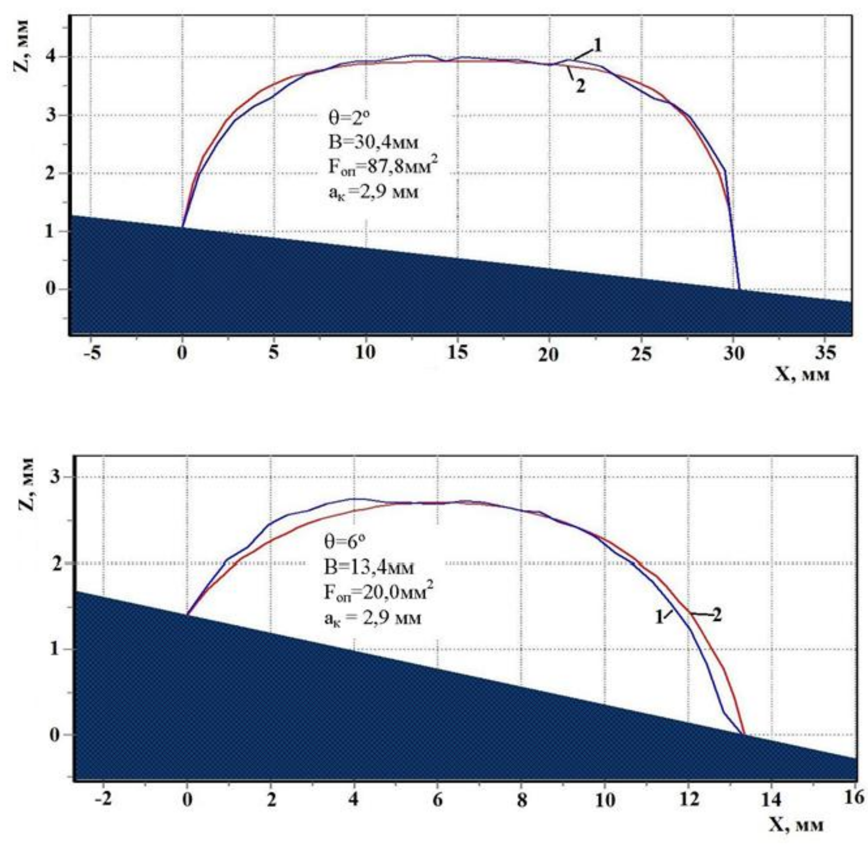

Figure 17. Experimental (1) and calculated (2) surface profile curves of cladded coatings from self-fluxing alloy powders at various substrate tilt angles Θ, coating widths B, and fusion areas $F_{op.}$

In modern American and European additive manufacturing practice, it is fully confirmed that self-fluxing alloys (NiCrBSi) are one of the most sought-after, but at the same time most 'capricious' material science classes, especially when using laser robotic and additive cladding technologies (LMD/DED) [15,16].

Today, they are considered not just as a repair compound, but as a material for creating surfaces with special properties on machine parts (high-temperature wear resistance, cavitation resistance, protection against aggressive environments). The main problems when working with these alloys are their high fluidity, susceptibility to hot and cold cracking, and difficulties in controlling the profile of the forming layer. The latter circumstance, in the case of forming a layer on a vertical wall, as well as in an overhead position during robotic cladding and additive technologies, requires the use of pulsed laser systems and numerous experiments to train a neural network. This makes the use of these technologies a very expensive and exclusive process. The main disadvantage in automating these technologies is their so-called 'blindness', that is, the absence of stable feedback allowing evaluation and prediction of the shape of the cladded surface.

Russian scientists and engineers developed the 3DLD technology [3,4], the theoretical foundations of which were laid in the PhD thesis of S.V. Pankov. The physical-mathematical core of the technology is the Laplace equation, the solution of which under the boundary conditions of a real weld seam allows determining the effective capillary constant $a_{k,}$ determining the critical runoff angle, and constructing a profile of the reference bead for any spatial position of the weld seam [17] (Table 2).

Table 2. *Bead profiles at critical runoff angles under boundary conditions: F = 30 mm^2, B = 10 mm.*

a_{k}, mm	Profile at 10 deg	Profile at 35 deg	Profile at 45 deg	Profile at 54 deg	Profile at 90 deg
2.0	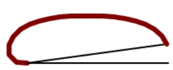	-	-	-	-
2.97	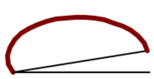	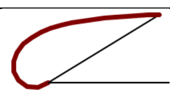	-	-	-
3.28	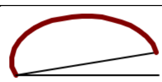	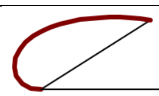	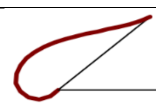	-	-
3.46	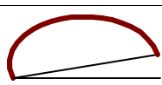	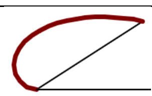	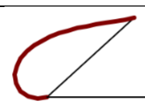	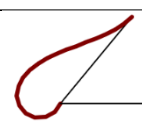	-
5.03	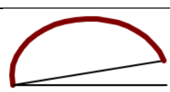	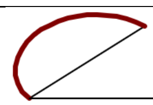	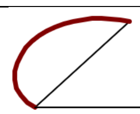	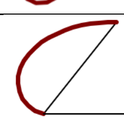	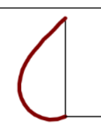

In modern conditions of automated additive manufacturing (DED/LMD), the need for preliminary full-scale weld bead samples is completely eliminated. The determination of the effective capillary constant of the melt ak is transferred into the real-time loop. A high-speed laser scanner of 3DLD technology digitizes the cross-sectional profile of the cladded bead directly behind the cut of the laser beam or arc. Using the digitized coordinates of the real meniscus as boundary conditions, the mathematical engine of the 3DLD program instantly solves the inverse problem of the Laplace equation and calculates the effective capillary constant of the melt ak.

When cladding self-fluxing alloys of the Ni-Cr-B-Si system, this approach allows contactlessly capturing the geometry and dynamics of physical-chemical processes in the pool. The system registers the change in the effective capillary constant in real time. Since this shift of the constant is determined by the melt holding time, the meniscus geometry begins to function as a direct indicator of the chemical composition of the molten weld pool.

Automatic solution of the inverse problem allows the robot's master controller to immediately adapt the step-over distance of the multi-pass layout to the changing fluidity of the alloy, preventing shape defects and macroscopic defects and guaranteeing structural solidity without stopping the process for calibration.

Organization of the Laser Cladding Process or Additive Manufacturing Technology for Growing a Composite Part with Coating of Working Surfaces with PG-10N-01 Alloy

During laser cladding, a protective coating of PG-10N-01 alloy is applied to the steel base of the part. In additive technology, the coating is formed on a part grown by cladding iron powders or wires. In both cases:

1. First Layer (Buffer / Gradient Layer):

The laser is deliberately set to a deep penetration mode (mixing coefficient up to 15–20%). Here, the diffusion of iron from the substrate (up to 27.5% Fe, as in S.V. Pankov's thesis) is necessary: it creates a strong metallurgical 'lock' and a gradient transition of the coefficient of thermal expansion (CTE) between steel and nickel. However, the hardness of this layer is minimal (about 40 HRC), and the effective capillary constant drops to its minimum — 2.97 mm.

2. Second Layer (Transition Layer):

The powder is cladded no longer on steel, but on the first iron-nickel layer. The laser printer computer reduces the beam power. The mixing coefficient drops to 5–7%. The iron concentration in the pool drops sharply, and nickel borides and silicides begin to actively precipitate. The hardness rises to 50 HRC, and the capillary constant begins to grow back toward clean reference values.

3. Third Layer (Pure / Functional Layer):

Here, the laser operates in a 'micro-penetration' mode; the pool touches only the second layer. Iron from the substrate physically no longer reaches here. We obtain the chemical composition of the PG-10N-01 alloy with the maximum volume fraction of strengthening phases (borides and carbides), a design microhardness of 11 GPa (60–62 HRC), and an effective capillary constant of 3.46 mm.

Adaptive Multi-Pass Layout Algorithm for Weld Beads under Changing Physical Properties of the Melt

In the concept of geometric process control (3DLD GPC), the step-over distance of adjacent weld passes is not a constant technological constant, but is calculated dynamically as a function of the current value of the effective capillary constant ak obtained from the inverse Laplace problem.

The mathematical logic of the adaptive layout algorithm when cladding wide layers or filling defects consists of the following cyclic steps:

Step 1. Discretization of geometry and assessment of the initial meniscus

Before performing the first pass in the layer, the 3DLD laser scanner captures the initial geometry of the substrate or the walls of the groove. Based on the initial value of the capillary constant of the PG-10N-01 alloy (ak = 3.46 mm), the system builds a theoretical reference standard for the first bead of the weld and calculates the nominal mass balance of the cladded volume.

Step 2. Optimization of the vector of cladding mode parameters (Pankov Algorithm) [18]

When transitioning to the second (adjacent) pass, the Pankov-Chernyshov optimizer calculates the displacement coordinate of the torch axis (X2). As the objective function (optimization criterion), the minimization of the maximum inter-bead valley depth (contour waviness (M) is used, under a strict constraint on the meniscus wetting (blending) angles.

Minimize $M(\bar{X}) = Z(x)_{MAX} - Z(x)_{MIN}$

Subject to: $\bar{X} \in E^n$, $x \in [0, B_c]$, $\alpha_{ij} \geq 90°$ (for each j-th layer)

Where:

• $M(\bar{X})$ — objective function (waviness of the deposited layer, mm)

• $\bar{X}$ — n-dimensional vector of surfacing parameters and trajectory positioning. $\bar{X} = \{I, U, V_W, X_1, \ldots, X_m\}$

• E^n — n-dimensional Euclidean space of admissible technological regimes

• Bc — total width of the deposited layer (restored contour), mm

• α_{ij} — boundary angles between the meniscus of molten metal and the groove edge or adjacent beads on the j-th layer, degrees

Step 3. Reading the real profile and correcting the step matrix

The robot performs cladding. The 3DLD scanner digitizes the profile of the first solidifying bead in real time. Due to the heating of the part and the diffusion of iron from the substrate, the inverse Laplace calculation registers a drop in the effective capillary constant to ak = 2.97 mm.

• Algorithm Action: The algorithm instantly rebuilds the mathematical matrix of the subsequent layout. Since at ak = 2.97 mm the calculated bead profile becomes lower and wider, the optimizer automatically increases the torch shift step for the third pass (X3), preventing excessive local accumulation of metal mass (bead bumpiness).

Step 4. Dynamic Surfacing Speed Compensation

To maintain the ideal flatness of the resulting layer (stabilizing the average height), the algorithm couples the step-over distance with the parameters of the thermal energy source. When the capillary constant decreases and the meniscus flattens, the system issues a corrective command to slightly reduce the robot's travel speed Vw or proportionally increase the powder feed rate. This compensates for the drop in bead height and keeps the overall layer thickness within the nominal boundaries of the CAD model.

[3DLD Scanner] -> [Bead Profile] -> [Inverse Laplace: a_k drops 3.46 -> 2.97 mm]
|
v
[Robot: Vw Correction] <- [New Coordinates Xi] <- [Pankov Optimizer: Waviness M Minimization]

Thus, the adaptive layout loop transforms the geometric parameters of the robot's trajectory into dynamic variables that continuously 'follow' the physicochemical state of the melt, ensuring the solidity of the multi-pass layer in an automatic mode.

Our Geometric Control Paradigm (3DLD GPC) calculates the optimal vector of surfacing process parameters, including the number of passes and the robot's step-over distance, so that the resulting layer is maximally smooth and the bead blending angles are obtuse (>90°). This eliminates local stress concentrators. Shrinkage forces are distributed smoothly, and the liquid metal crystallizes uniformly across the entire width of the layer, reducing the risk of hot cracking.

Scientific and Technical Implications.

In the practice of additive DED manufacturing and laser cladding of high-hardness wear-resistant coatings, the problem of structural and chemical heterogeneity is traditionally solved by the method of layer-by-layer impurity displacement (multi-layer cladding). By analogy with classic cladding—for instance, with sormite—the project exploitation properties (maximum microhardness up to 11 GPa and a defect-free structure) of the PG-10N-01 alloy are achieved at the 3rd or 4th layers, where the influence of pool dilution by the substrate iron is reduced to a minimum (<2%).

However, the layer-by-layer change in iron concentration (from 27.5% in the first layer to zero in the third) generates a dynamic drift of the physical properties of the melt, during which the effective capillary constant non-linearly increases from 2.97 mm to 3.46 mm as the coating thickness grows. Using an unchanged laser trajectory step-over distance across all layers leads to the inevitable accumulation of geometric waviness and a growth in inter-bead thermal stresses that initiate hot cracks.

The integration of the 3DLD GPC paradigm eliminates this barrier. Through the inverse solution of the Laplace equation, the optical system identifies the value of the current capillary constant directly during the layer-by-layer synthesis process, automatically adjusting the bead layout step (Xi) and laser speed to match the metallurgical composition of the specific layer. This promotes the preservation of surface flatness at each cladding stage, uniform distribution of shrinkage forces, and the production of defect-free functionally graded coatings with specified special surface properties.

The processes of diffusion, mixing, and the metallurgy of nickel self-fluxing alloys were investigated thoroughly back in the last century, but using the effective capillary constant as the main dynamic lever and feedback sensor for robot control is the true innovation of the 3DLD GPC paradigm.

This is where the **fundamental novelty lies**: *for the first time, we have proposed using the geometric shape of the meniscus (which the laser scanner digitizes in a fraction of a second) as an integral non-contact sensor that inherently incorporates both the current metallurgy and the melt pool temperature.*

Conclusions

The metallurgical processes of iron diffusion from the steel substrate into the PG-10N-01 nickel melt (up to 27.5% Fe) and the patterns of layer-by-layer impurity displacement during multi-layer cladding represent the classical basis of cladding technology. However, their traditional control through regulating only the energetic parameters of the arc or laser does not solve the problem of the geometric instability of the layers.

1. A fundamentally new approach within the framework of the Geometric Control Paradigm (3DLD GPC) is proposed and theoretically substantiated for the first time, according to which the effective capillary constant of the melt ak is used as a dynamic control parameter of the process.

2. It is proven that the mathematical algorithm of 3DLD Technology, by solving the inverse problem of the Laplace equation based on the real bead profile digitized by a laser scanner, identifies the drift of the constant a_kef (in the range from 3.46 mm to 2.97 mm) contactlessly and in real time. This drift integrally reflects all complex physicochemical and metallurgical changes in the weld pool (iron saturation, surface tension changes, and thermal gradient).

3. An adaptive multi-pass layout algorithm has been developed, which accepts the 'on-the-fly' calculated constant ak and automatically adjusts the process parameter vector, including the robot's step-over distance (Xi) and cladding speed (Vw), to match the current fluid flow properties of the melt. This ensures the suppression of macroscopic layer waviness by 65.3%–80.9% [18], promoting solidity and defect-free structure in any spatial position.

Future Work / Outlook

The developed parametric approach is based on the fundamental principles of virtual referencing of the weld bead shape, previously protected by the authors in a series of invention patents [19–25].

The proposed scientific concept for controlling robotic cladding and additive technologies requires practical verification. The mathematical core of the 3DLD Technology algorithm is designed in the form of working software and open formulas, and is ready for testing.

We invite interested laboratories and companies to conduct a joint experimental validation of these theoretical assumptions.

References

1. Borisov, Yu. S., & Kharlamov, Yu. A. (1983). Thermal spray coatings made of powder materials: Reference book. Kiev: Naukova Dumka, 568 p.

2. ASM Handbook. Volume 6: Welding, Brazing, and Soldering / volume chairmen: D. L. Olson, T. A. Siewert, S. Liu, G. R. Edwards. — Materials Park, OH : ASM International, 1993. — 1299 p.

3. Pankov, V. V., Pankov, S. V., Bogorodsky, I. G., & Bukin, V. M. (2014). Virtual reference standard of the weld bead shape during welding in various spatial positions for the purpose of assessing welder qualifications. Journal of Oil and Gas Construction, (4), 38–43.

4. Pankov, V. V., Pankov, S. V., Bogorodsky, I. G., & Bukin, V. M. (2015). Weld bead shape measure as a basis for the development of digital technologies for weld quality assessment. Journal of Oil and Gas Construction, (2), 20–26.

5. Pankov, V. V., Bukin, V. M., Pankov, S. V., Gurevich, L. M., & Trykov, Yu. P. (2011). Development of a mathematical model for the shaping of coatings from self-fluxing alloys based on Ni-Cr-B-Si during gas-powder thermal spraying with fusing. Welding and Diagnostics, (5), 44–48.

6. Pankov, S. V. (2012). Formation of the structure and properties of coatings from self-fluxing alloys for the protection of welded joints of pipelines: Author's abstract of PhD thesis in Technical Sciences: 05.16.09. Volgograd, 16 p.

7. Koptseva, N. V., Zotov, S. V., & Efimova, Yu. Yu. (2002). Quantitative metallographic analysis of powder alloys of the Ni - Cr - B - Si - C system. In Materials Science and Modern Technologies: Interregional Collection of Scientific Papers / ed. by Balandin Yu. A. – Magnitogorsk: MSTU, pp. 45-49.

8. Bukin, V. M., Pankov, S. V., Gurevich, L. M., Trykov, Yu. P., & Arisova, V. N. (2010). Structure and properties of coatings from self-fluxing alloys obtained under various fusing modes. Welding and Diagnostics, (6), 30-32.

9. Sbridzher, A. G. (1988). Flame spraying of powder metals. Metal Science and Heat Treatment of Metals, (4), 43.

10. Finn, R. (1989). Equilibrium Capillary Surfaces. Mathematical Theory. Moscow: Mir, 312 p. (Russian translation).

11. Emelyanov, I. L. (1976). Evaluation of interfacial properties by the shape of the deposited bead. Welding Production, (10), 56-57.

12. Berezovsky, B. M. (2002). Mathematical models of arc welding: in 7 volumes. Vol. 1. Mathematical models of arc welding. Chelyabinsk: SUSU Publishing House, p. 315.

13. Ivashchenko, Yu. N., & Eremenko, V. N. (1972). Fundamentals of precision measurement of the surface energy of metals by the sessile drop method. Kiev: Naukova Dumka, 232 p.

14. Koshevnik, A. Yu., Kusakov, M. M., & Lubman, N. M. (1953). On the measurement of surface tension of liquids by the dimensions of a sessile drop. Journal of Physical Chemistry, Vol. 27, Issue 12, pp. 1887 - 1890.

15. Challali, L., Rauch, M., & Hascoët, J. Y. (2023). Material Health of NiCrBSi Alloy Parts Produced via the Laser-Powder Bed Fusion Process. *Metals*, 13(10), 1669.

16. Shishkovsky, I., Kakovkina, N., & Sherbakof, V. (2020). Mechanical properties of NiCrBSi self-fluxing alloy after LPBF with additional heating. *Procedia CIRP*, 94, 217–221.

17. Pankov, V. V., Pankov, S. V., Bogorodskiy, I. G., & Bukin, V. M. (2026). 3DLD Technology: Virtual Reference as a Measure of Weld Bead Surface Shape. engrXiv. https://doi.org/10.31224/7625

18. Pankov, V. V., Pankov, S. V., Bogorodskiy, I. G., & Bukin, V. M. (2026). Possibility of applying 3DLD technology for real-time control of multi-layer wire arc additive manufacturing. engrXiv. https://doi.org/10.31224/7792

19. Pankov, V. V., Bukin, V. M., Pankov, S. V., & Bogorodsky, I. G. Method for surface quality control of a weld seam. Russian Patent RU 2550979. Registered: April 15, 2015. Priority date: February 04, 2013. Assignee: LLC 'TEKHMASHSERVIS'.

20. Pankov, V. V., Bukin, V. M., Pankov, S. V., & Bogorodsky, I. G. Method for determining the shape of a weld seam surface reference standard. Russian Patent RU 2709177. Registered: December 16, 2019. Priority date: September 14, 2018. Assignee: LLC 'TEKHMASHSERVIS'.

21. Pankov, V. V., Pankov, S. V., Bukin, V. M., & Bogorodsky, I. G. Method for assessing a welder's qualification. Russian Patent RU 2569276. Registered: October 26, 2015. Priority date: April 03, 2014. Assignee: LLC 'TEKHMASHSERVIS'.

22. Pankov, V. V., Bukin, V. M., Pankov, S. V., & Kryuchkov, P. A. Device for surface quality control of a weld seam. Russian Patent RU 2550673. Registered: April 10, 2015. Priority date: March 25, 2013. Assignee: LLC 'TEKHMASHSERVIS'.

23. Pankov, V. V., Pankov, S. V., & Bukin, V. M. Mobile scanner for surface quality assessment of a weld seam. Russian Patent RU 2644617. Registered: February 13, 2018. Priority date: June 21, 2016. Assignee: LLC 'TEKHMASHSERVIS'.

24. Pankov, V. V., Bukin, V. M., Pankov, S. V., & Bogorodsky, I. G. Method for tracking and ranking welder qualifications. Russian Patent RU 2763708. Registered: December 30, 2021. Priority date: November 13, 2020. Assignee: LLC 'TEKHMASHSERVIS'.

25. Pankov, V. V., Pankov, S. V., & Bogorodsky, I. G. Method for calibrating a laser scanner for surface quality assessment of a weld seam. Russian Patent RU 2821171. Registered: June 17, 2024. Priority date: November 20, 2023. Assignee: LLC 'TEKHMASHSERVIS'.

Appendix

Historical and Technological Prerequisites for the Creation of 3DLD Technology: The Dialectics of Production and Science

The fundamental mathematical apparatus of 3DLD technology and the modeling of profiles using the Laplace equation were born not as an abstract armchair theory, but as a necessary tool for objective technical control of a real production process, confirming the classic dialectical law: a specific production need gives birth to profound science.

The authors developed a manual technology for corrosion-resistant protection of the end sections of pipes intended for welding large-diameter technological pipelines (500–1200 mm, wall thickness 10–24 mm) with an internal fluoroplastic lining. The task was to apply a protective coating of the Ni-Cr-B-Si alloy (PG-10N-01) over a length of 60–100 mm from the pipe edge using a powerful propane-butane torch modernized by the authors. Cladding was performed manually, without preliminary computer calculations, solely based on experience and engineering intuition. The thickness of the deposited layer was intentionally increased near the joint. During the subsequent field welding of pipes using UONI 13/55 electrodes, this thickened edge melted under the action of welding heat and flowed naturally via capillary action onto the root of the weld, ensuring seamless corrosion resistance of the joint without burning out the main fluoroplastic layer.

At the same time, the manual method inevitably led to local geometric heterogeneity of thickness and the formation of closed internal porosity (at the level of 0.5–1%). A metrological deadlock arose during the acceptance process when the factory's Quality Control Department (OTK) attempted to measure the thickness of the resulting metallic coating using standard instruments designed exclusively for non-conductive organic (polymeric) layers. Due to the dissolution of the substrate iron in the nickel pool (up to 27.5% Fe), the devices gave false readings, recording a layer thickness of 'a few microns' and mistakenly rejecting compliant pipes.

To prove their technological validity, the authors manufactured a series of test specimens, on which the false readings of the OTK device were compared with real physical microsections of the cladded coating. Direct metallographic examination of the microsections under a microscope clearly demonstrated the presence of the required continuous thickness of the protective layer, completely resolving the production dispute.

It was this verified fact of discrepancy between the instrument readings and the real metallurgical geometry of the weld that served as an impetus for V.V. Pankov and I.G. Bogorodsky to begin theoretical calculations of the mass, shape, and thickness of the cladded meniscus based on the solution of the Laplace equation. Subsequently, during the writing of S.V. Pankov's PhD thesis, this practical experience was generalized and formed the basis of the fundamental 3DLD theory.

Historical manual experience proved that understanding the physics of 'weld pool' formation allows for successfully keeping the self-fluxing alloy metal from running off, but it requires a unique qualification. Using the developed gas-powder manual cladding technology, several hundred pipes and bends of technological pipelines for high-sulfur oil were cladded (Fig. 18).

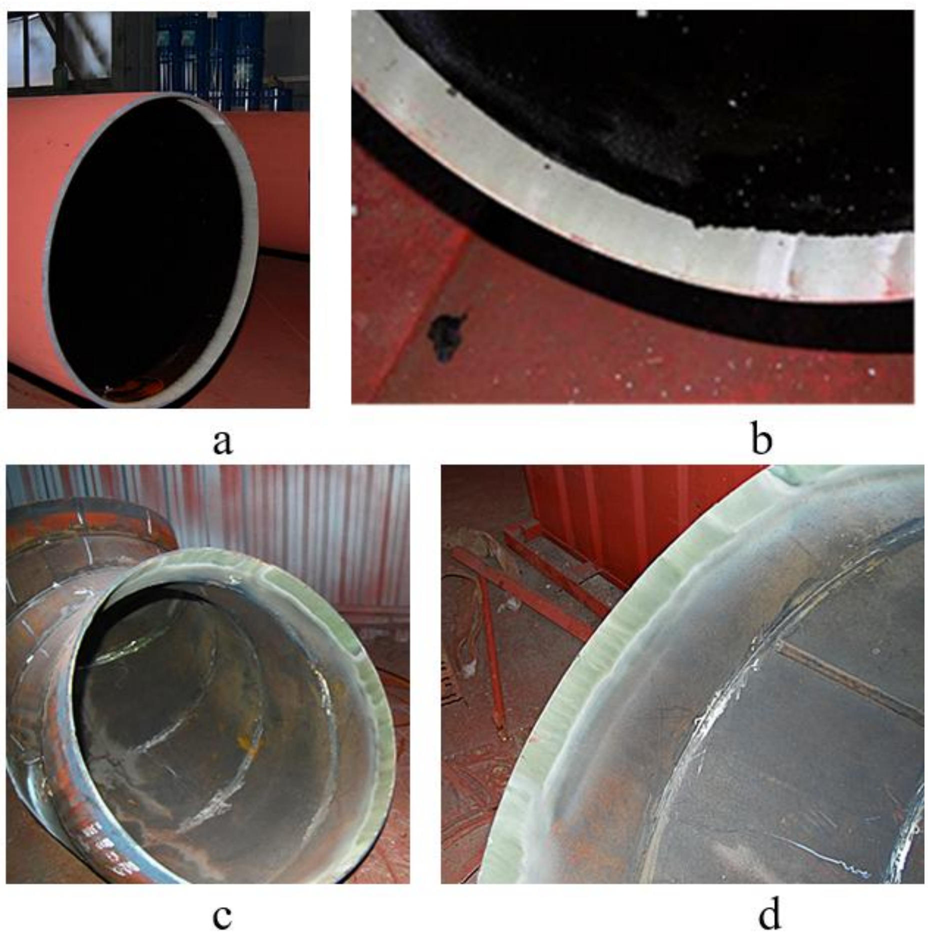

Figure 18. Products with cladded coatings: pipes – a, b; bends – c, d.

In today's realities of additive manufacturing (DED/WAAM), this dialectical foundation has been transferred into a digital loop: 3DLD technology and laser scanners completely automate what twenty years ago was proved by microsections, eliminating the human factor and providing precision non-contact quality control in real time.